Nanoscale

PAPER

View Article Online
View Journal | View Issue

Cite this: *Nanoscale*, 2014, **6**, 8949

CVD synthesis of large-area, highly crystalline $MoSe_2$ atomic layers on diverse substrates and application to photodetectors†

Jing Xia,[a] Xing Huang,[ab] Ling-Zhi Liu,[c] Meng Wang,[a] Lei Wang,[a] Ben Huang,[a] Dan-Dan Zhu,[a] Jun-Jie Li,[c] Chang-Zhi Gu[c] and Xiang-Min Meng*[a]

Received 29th April 2014
Accepted 30th May 2014

DOI: 10.1039/c4nr02311k

www.rsc.org/nanoscale

Synthesis of large-area, atomically thin transition metal dichalcogenides (TMDs) on diverse substrates is of central importance for the large-scale fabrication of flexible devices and heterojunction-based devices. In this work, we successfully synthesized a large area of highly-crystalline $MoSe_2$ atomic layers on SiO_2/Si, mica and Si substrates using a simple chemical vapour deposition (CVD) method at atmospheric pressure. Atomic force microscopy (AFM) and Raman spectroscopy reveal that the as-grown ultrathin $MoSe_2$ layers change from a single layer to a few layers. Photoluminescence (PL) spectroscopy demonstrates that while the multi-layer $MoSe_2$ shows weak emission peaks, the monolayer has a much stronger emission peak at ~1.56 eV, indicating the transition from an indirect to a direct bandgap. Transmission electron microscopy (TEM) analysis confirms the single-crystallinity of $MoSe_2$ layers with a hexagonal structure. In addition, the photoresponse performance of photodetectors based on $MoSe_2$ monolayer was studied for the first time. The devices exhibit a rapid response of ~60 ms and a good photoresponsivity of ~13 mA/W (using a 532 nm laser at an intensity of 1 mW mm^{-2} and a bias of 10 V), suggesting that $MoSe_2$ monolayer is a promising material for photodetection applications.

1. Introduction

The experimental realization of graphene has triggered a worldwide upsurge in research interest on other two-dimensional (2D) layered materials such as VS_2, CoS_2, GaSe, h-BN and $NbSe_2$.[1–7] These 2D crystals exhibit a variety of electrical characteristics including metallic, semimetallic, semiconducting, insulating, and charge density wave behaviour. In particular, atomically-thin group-VIB transition metal dichalcogenides (TMDs) (MX_2; M = W, Mo; X = S, Se) are a new class of 2D semiconductors with extraordinary properties and tremendous application potential.[8–11] For example, while the bulk of TMDs have an indirect bandgap, the monolayers show a sizable direct bandgap around 1–2 eV, making them appealing materials for ultrathin, lightweight, and flexible device applications such as field effect transistors (FETs), photovoltaic cells, light emitting diodes (LEDs) and photodetectors.[8,12–15] Interestingly, the electronic structures of these materials can be effectively modulated by partially substituting the metal or nonmetal atoms with their congeners, forming 2D TMD alloys ($Mo_{1-x}W_xS_2$, $Mo_{1-x}W_xSe_2$, $MoS_{2(1-x)}Se_{2x}$, *etc.*).[16–19] The availability of various alloys with tunable bandgaps will not only promote fundamental studies of these materials, but will also allow their practical application in electronics and optics. Recent studies have demonstrated that the breaking of inversion symmetry together with the spin-orbit interaction could result in the coupling of spin and valley physics in monolayer TMDs, making it possible to manipulate the spin and valley degrees of freedom in these novel 2D crystals.[20–22]

Until now, most studies on group-VIB TMDs have concentrated on MoS_2. Other group-VIB TMDs such as $MoSe_2$, however, possess attractive properties. For instance, monolayer $MoSe_2$ has a direct bandgap of ~1.5 eV, which is close to the optimal bandgap value of single-junction solar cells and photoelectrochemical cells.[23,24] Few-layer $MoSe_2$ has nearly degenerate indirect and direct bandgaps, and an increase in temperature can effectively push the system towards the 2D limit.[24] In contrast to MoS_2, monolayer $MoSe_2$ has a larger spin-splitting energy of ~180 meV at the top of the valence bands, which makes $MoSe_2$ more applicable than MoS_2 in spintronics.[25,26] While some methods including exfoliation (chemical or mechanical) from the bulk,[27–29] hydrothermal synthesis,[27,30] and selenization of metals[31,32] have been used to produce $MoSe_2$ nanosheets, none of these approaches are able

[a]*Key Laboratory of Photochemical Conversion and Optoelectronic Materials, Technical Institute of Physics and Chemistry, Chinese Academy of Sciences, Beijing, 100190, P.R. China. E-mail: mengxiangmin@mail.ipc.ac.cn*

[b]*Department of Inorganic Chemistry, Fritz Haber Institute of the Max Planck Society, Faradayweg 4-6, 14195 Berlin, Germany*

[c]*Beijing National Laboratory of Condensed Matter Physics, Institute of Physics, Chinese Academy of Sciences, Beijing, 100190, China*

† Electronic supplementary information (ESI) available: AFM images and height profile of bilayer and trilayer $MoSe_2$ flakes; A direct transfer method used for preparation of $MoSe_2$ TEM samples. See DOI: 10.1039/c4nr02311k

to synthesize large-area, uniform, and highly-crystalline $MoSe_2$ atomic layers. Although molecular beam epitaxy (MBE) is a facile method to grow large-scale ultrathin $MoSe_2$ layers of high quality,[26] it is not suitable for industrial production because of its high cost. Until recently, CVD has been used to successfully grow large-area ultrathin $MoSe_2$ layers on SiO_2/Si substrates.[33–35]

For different applications such as flexible devices[36–39] and heterojunction-based devices,[40–43] however, the growth of $MoSe_2$ atomic layers on SiO_2/Si substrates is not sufficient; different functionalities require the integration of $MoSe_2$ with different kinds of materials. Therefore, the synthesis of large-scale, high-quality, ultrathin $MoSe_2$ layers on diverse substrates is necessary. To this end, we herein report a simple CVD method to directly grow a large area of highly-crystalline $MoSe_2$ atomic layers on SiO_2/Si, mica and Si substrates at atmospheric pressure using MoO_3 and Se powders as starting materials. Scanning electron microscopy (SEM), optical microscopy (OM), AFM, Raman spectroscopy, PL spectroscopy, and TEM have been used to systematically study the samples. In addition, photodetectors based on monolayer $MoSe_2$ were fabricated and studied for the first time. The devices exhibited a fast response and a good photoresponsivity.

2. Experimental section

Growth of $MoSe_2$ atomic layers

We obtained $MoSe_2$ layers by the selenization of MoO_3 powder (99.99%, Beijing Lanyi Chemical Co., Ltd) in a high temperature CVD furnace (GSL-1400X tube furnace, Hefei Kejing Material Technology Co., Ltd). In a typical CVD growth, a ceramic boat containing 10 mg of MoO_3 powder located at the centre of the heating zone and another ceramic boat with 0.5 g of Se powder (99.99%, Beijing Lanyi Chemical Co., Ltd) located upstream of the furnace 10–20 cm away from the MoO_3 powder were placed in the furnace. Cleaned 300 nm SiO_2/Si, mica and the newly-cleaved side-wall of SiO_2/Si substrates were placed downstream close to the MoO_3 powder along the quartz tube. The furnace chamber was vacuum pumped to expel the air and then filled with high-purity Ar to atmospheric pressure. Next, the centre of the heating zone was heated to 820 °C within 41 min and kept for 15 min before being allowed to cool naturally. During the growth process, high-purity Ar with a flow rate of 10 standard cubic centimeters per minute (sccm) was used as the gas carrier.

Characterization

SEM characterization was carried out on a Hitachi S-4800 with an acceleration voltage of 5–10 kV. Optical images were obtained using an optical microscope (Nikon Inverted Microscope Eclipse Ti-U with a CCD of Nikon Digital Sight). The thickness profile was determined using an atomic force microscope (Veeco Nanoscope V) at a scanning rate of 0.976 Hz with 512 scanning lines. Raman spectra and PL spectra were recorded with a Renishaw InVia Raman microscope with a 50× objective. The Si peak at 520 cm^{-1} was used as a reference for wavenumber calibration. For the Raman and PL measurements, we used a 532 nm laser and an 1800 I mm^{-1} grating. The laser was focused on the sample at a power of ~250 μW to minimize the laser-induced thermal effect. The structure and composition of $MoSe_2$ samples were investigated by a JEOL JEM-2100F at an acceleration voltage of 200 kV and energy dispersive X-ray spectroscopy. For TEM characterization, an ultrathin carbon film supported on a copper grid was used. The method for transferring the $MoSe_2$ sample is similar to that in the previous report on the direct transfer of graphene.[44] In our experiments, we didn't wet the sample with isopropanol; instead, 1% HF solution was used directly as the etchant. The detailed procedures are shown in ESI Fig. S2.†

Photodetectors based on monolayer $MoSe_2$ were fabricated by evaporating 100 nm Au directly on the top of $MoSe_2$ layers patterned by electron beam lithography (Raith 150). Photocurrent measurement was performed at room temperature under atmospheric conditions. The illuminating 532 nm laser was generated by Spectra-Physics Laser. A laser attenuator was used to obtain different laser intensities, which were confirmed by a laser power meter. The electrical measurement was carried out using a Keithley-4200SCS semiconductor parameter analyser.

3. Results and discussion

In this work, a high-temperature tube furnace was used for the CVD synthesis of $MoSe_2$ atomic layers; the schematic representation of the growth setup is displayed in Fig. 1a. During the CVD growth, the centre of the heating zone was heated to 820 °C under Ar atmosphere (see details in the experimental section). At such a high temperature, MoO_3 powder was partially reduced by Se vapour to form volatile suboxide MoO_{3-x} species that were transported downstream by the Ar carrier gas.[45] Selenization of vapour-phase MoO_{3-x} could then produce $MoSe_2$ species, which nucleated on the substrate and grew into large $MoSe_2$ atomic

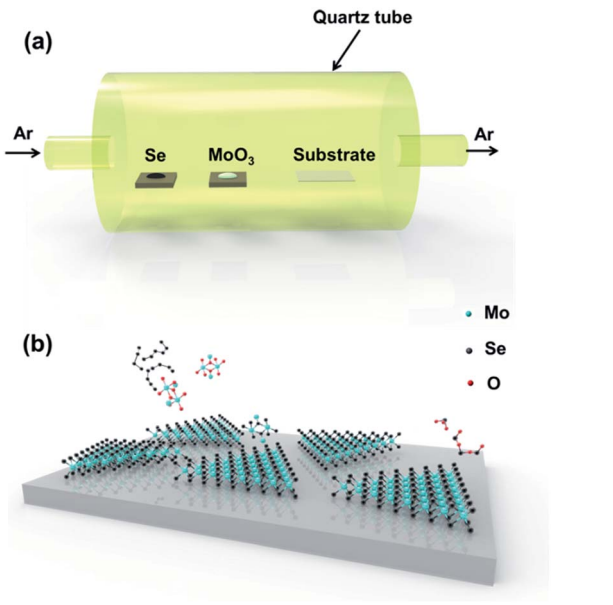

Fig. 1 (a) Growth setup for synthesizing $MoSe_2$ atomic layers. (b) A schematic view illustrating the growth of $MoSe_2$ layers.

layers.[45–47] The corresponding schematic is illustrated in Fig. 1b. Recent reports on the growth of $MoSe_2$ atomic layers have used a similar CVD approach.[33–35] In their syntheses, the growth was performed at 750 °C or 800 °C under an Ar–H_2 gas mixture environment in which H_2 gas acted as an indispensable reducing agent. Interestingly, in our method, the CVD growth could take place efficiently without the use of H_2.

Fig. 2a–c show typical SEM images of large-area $MoSe_2$ layers grown on SiO_2/Si, mica and Si substrates, respectively. The spatial distribution of $MoSe_2$ layers (darker contrast in Fig. 2a–c) indicates that $MoSe_2$ nucleates randomly on the substrates. For samples grown on SiO_2/Si and mica substrates, most of the isolated $MoSe_2$ islands have equilateral triangle morphologies with edge lengths ranging from a few microns to 40 μm (Fig. 2a and b), suggesting the single crystalline nature of these domains.[35,48] In contrast, $MoSe_2$ layers synthesized on the cleaved side-wall of SiO_2/Si substrates show irregular shapes with sizes larger than 50 μm (Fig. 2c). This result indicates that the substrates have an important influence on the morphology of TMDs.[48,49]

Fig. 2d and e display OM images of $MoSe_2$ layers grown on SiO_2/Si and mica substrates, respectively. The sharp colour contrast between the triangular crystallites (greyish triangular flakes in Fig. 2d; white triangular flakes in Fig. 2e) and the substrates (violet area is the bare SiO_2/Si substrate in Fig. 2d; black regions represent the mica in Fig. 2e) demonstrates the high uniformity of the $MoSe_2$ domains. The thickness-dependent contrast observed in the OM images reveals single- , bi- , tri- and multi-layered $MoSe_2$ flakes, as marked in Fig. 2d. To determine the thicknesses of these $MoSe_2$ layers, they were characterized with AFM. Fig. 2f shows the AFM image and height profile of a monolayer $MoSe_2$ triangle. The homogeneous colour contrast signifies that this flake has a flat and uniform surface, and its thickness (0.71 nm) confirms that this $MoSe_2$ triangular flake is a monolayer.[24,29] AFM images and height profiles are also shown for bilayer and trilayer $MoSe_2$ (Fig. S1†).

In order to investigate the crystal structure of the $MoSe_2$ flakes, a direct transfer approach was used to prepare TEM samples. The approach is not only suitable for 2D $MoSe_2$, but also other 2D crystals such as MoS_2, WS_2 and WSe_2 grown on SiO_2/Si, mica and Si substrates. Unlike PMMA-assisted transfer technology,[35] the direct transfer method is much more rapid and convenient. The detailed procedure can be found in Fig. S2.† Fig. 3a displays a bright-field TEM image of a monolayer $MoSe_2$ triangular flake with an edge length of ~3.5 μm. The lattice fringe measured from the high-resolution TEM

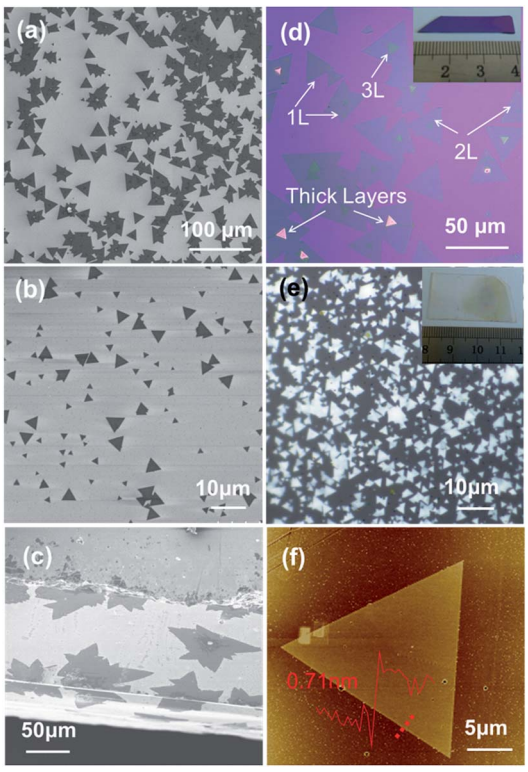

Fig. 2 SEM images of $MoSe_2$ layers synthesized on (a) SiO_2/Si, (b) mica and (c) Si substrates. (d) Optical image of $MoSe_2$ layers on a SiO_2/Si substrate. The violet area is the bare SiO_2/Si substrate; the greyish, light green and pink triangles represent $MoSe_2$. The inset shows a photograph of 2D $MoSe_2$ grown on the SiO_2/Si substrate. (e) Optical image of $MoSe_2$ layers on a mica substrate. The inset shows a photograph of 2D $MoSe_2$ grown on the mica substrate. White triangular flakes represent $MoSe_2$; the black area is the mica. (f) AFM image and height profile of an $MoSe_2$ monolayer.

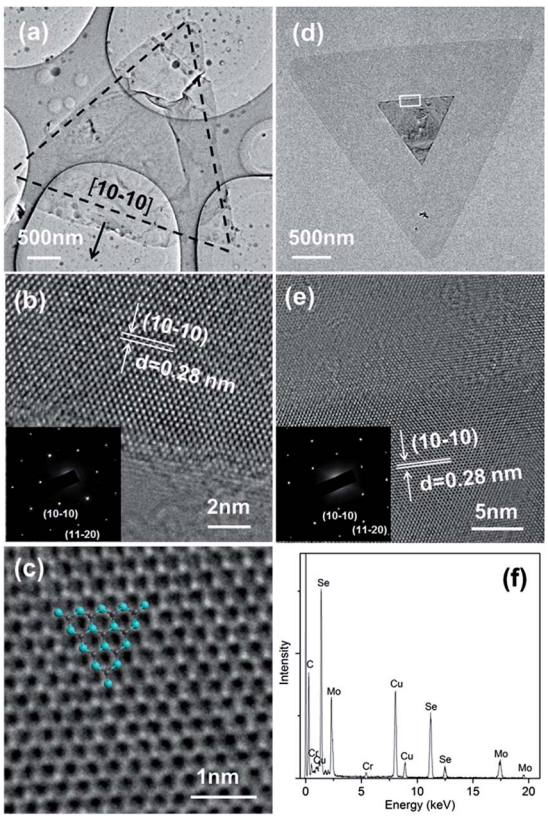

Fig. 3 (a) Bright-field TEM image of a monolayer $MoSe_2$ triangle. (b) HRTEM image of the $MoSe_2$ triangle. The inset shows the SAED pattern. (c) HRTEM phase-contrast image of the $MoSe_2$ triangle. The inset shows the hexagonal arrangement of Mo and Se atoms. (d) Bright-field TEM image of a few-layer $MoSe_2$ triangle. (e) HRTEM image and corresponding SAED pattern of the marked region in Fig. 3d. (f) EDX spectrum of the $MoSe_2$ layers.

(HRTEM) image in Fig. 3b is 0.28 nm, corresponding to the $\{10\bar{1}0\}$ planes. The selected area electron diffraction (SAED) pattern (inset in Fig. 3b) from the $MoSe_2$ triangle exhibits one set of six-fold symmetry diffraction spots, confirming the single-crystalline nature of this flake with a hexagonal structure. By analysing the HRTEM image in Fig. 3b, we see that the edge of the $MoSe_2$ triangle is perpendicular to the $[10\bar{1}0]$ direction, indicating that the sample has zigzag edges.[50,51] The HRTEM phase-contrast image (Fig. 3c) of the $MoSe_2$ triangle shows a honeycomb-like structure, which is consistent with previous reports.[47,51]

Few-layer $MoSe_2$ was characterized in addition to monolayer $MoSe_2$ (Fig. 3d and e). The bright-field TEM image in Fig. 3d shows a few-layer $MoSe_2$ triangle with a small triangular island on the top. Intriguingly, the small triangular island is located both at the centre of the bottom triangle and parallel to it, indicating an AB stacking growth mode.[33,52] The HRTEM image of the marked region in Fig. 3d is displayed in Fig. 3e. The interface between adjacent layers can be distinguished due to the contrast difference. The corresponding SAED pattern in Fig. 3e demonstrates the single-crystallinity of the few-layer $MoSe_2$ with a hexagonal structure. Furthermore, energy dispersive X-ray spectroscopy (EDX) equipped in TEM was applied to study the composition of the $MoSe_2$ samples. As shown in Fig. 4f, the intense peaks of Mo and Se confirm that MoO_3 has been successfully converted into $MoSe_2$.

The as-synthesized $MoSe_2$ layers were further investigated by Raman spectroscopy using a 532 nm excitation laser (Fig. 4a). Two typical Raman active modes, *i.e.*, the prominent A_{1g} Raman mode and the weak E_{2g} Raman mode, are observed in the Raman spectra. The A_{1g} mode relates to the out-of-plane vibration of Se atoms, and the E_{2g} mode is associated with the in-plane vibration of Mo and Se atoms (see the inset in Fig. 4a). In general, the location of Raman modes can be used to determine the thickness of 2D materials.[6,45,53] In this study, the A_{1g} and E_{2g} modes of single-layer $MoSe_2$ are located at 240.6 cm^{-1} and 287.5 cm^{-1}, respectively (Fig. 4a). As the layer thickness increases, the A_{1g} Raman mode is blueshifted to 242.3 cm^{-1} for 2–3L, and to 243.9 cm^{-1} for thick $MoSe_2$; the E_{2g} Raman mode exhibits a redshift to 285.9 cm^{-1} for $\geq$2L. The stiffening of the A_{1g} mode may result from the increasing van der Waals interaction between layers, while the softening of the E_{2g} mode may be caused by the presence of long-range coulomb interactions between layers.[54–56] Similar phenomena have been previously reported in other 2D materials including graphene, h-BN, MoS_2 and GaSe.[5,6,45,53] The frequency difference between the E_{2g} and A_{1g} modes is another important indicator of the thickness of 2D materials, although different substrates may have an effect. In our case, the peak spacing between E_{2g} and A_{1g} modes decreases as the layer number increases. The spacings are 46.9 cm^{-1}, 43.6 cm^{-1} and 42 cm^{-1} for $MoSe_2$ monolayers, 2–3L and thick samples, respectively.

Recent studies have demonstrated that the electronic structure of $MoSe_2$ varies with its thickness.[8,11] To confirm this behaviour in the CVD-grown samples, PL experiments (532 nm laser) were carried out. Fig. 4b shows the room-temperature PL spectra of $MoSe_2$ layers of different thicknesses. It can be seen that

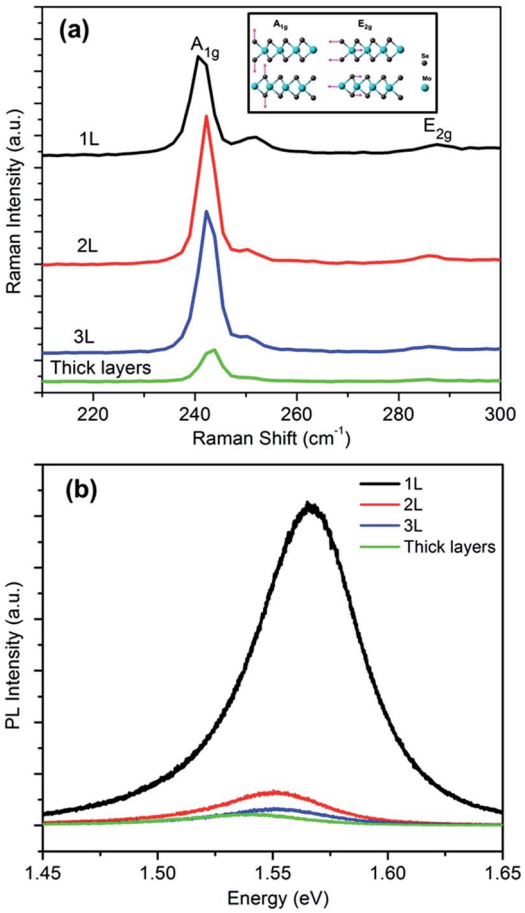

Fig. 4 (a) Raman spectra of $MoSe_2$ layers with different thicknesses. The inset shows schematic representations of the A_{1g} and E_{2g} modes. (b) Room-temperature PL spectra of $MoSe_2$ layers with different thicknesses.

monolayer $MoSe_2$ exhibits a single emission peak at ~1.56 eV with a very strong PL intensity; which can be ascribed to the direct bandgap at the K high symmetry point of the Brillouin zone.[24] With increasing layer number, PL intensity declines sharply. For example, the PL intensity of bilayer $MoSe_2$ is approximately 10-times weaker than that of the monolayer (Fig. 4b). As the thickness increases, the PL peak is also redshifted to ~1.54 eV for thick $MoSe_2$ layers. The change in PL intensity and bandgap should be attributed to the transition from direct to indirect bandgap, which has been previously reported.[24] Generally, Raman spectra and PL spectra demonstrate the high quality of the as-grown $MoSe_2$ atomic layers in this study.

Due to its sizeable direct bandgap of ~1.56 eV, monolayer $MoSe_2$ could be a promising candidate for photodetection applications. In view of this, photodetectors based on monolayer $MoSe_2$ were fabricated using electron beam lithography and metal evaporation, as illustrated schematically in Fig. 5a. In this study, Au was used as the metal electrode due to its large work function.[57,58] In general, 100 nm of Au was deposited on the top of the $MoSe_2$ monolayers by electron beam evaporation. The as-fabricated devices were then annealed at 200 °C for 2 h in an Ar atmosphere to improve the contact.

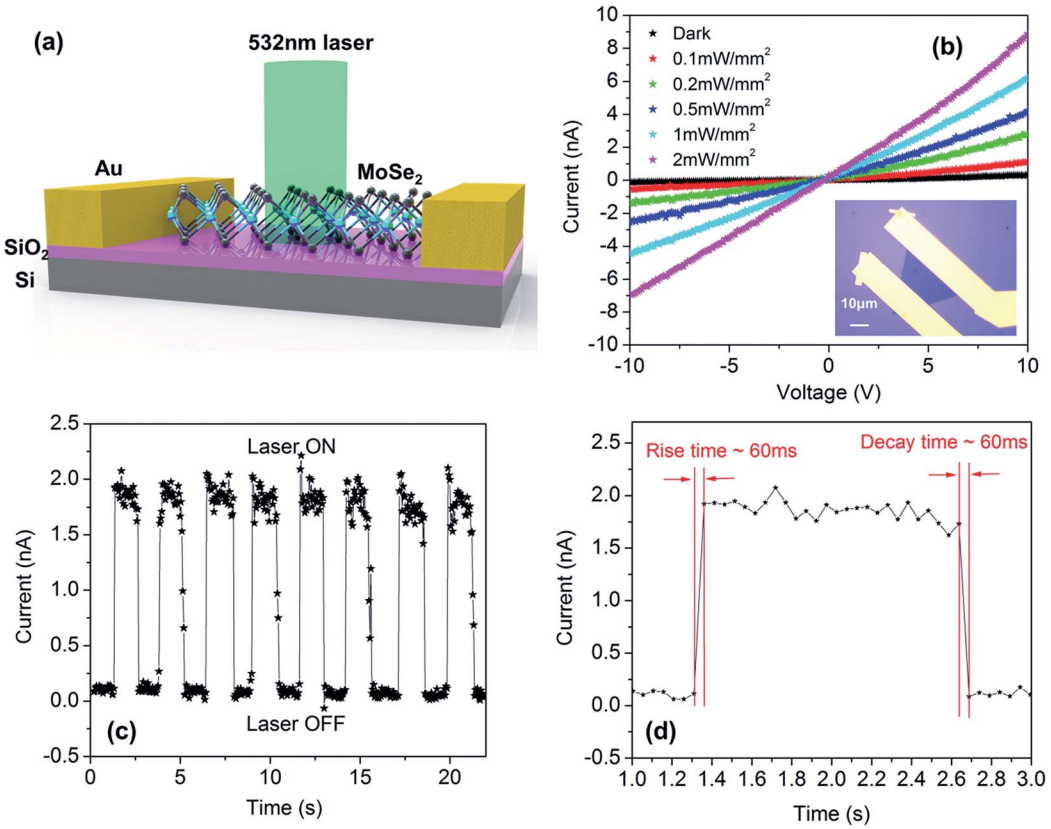

Fig. 5 (a) Three-dimensional schematic view of a monolayer $MoSe_2$ photodetector and the 532 nm laser beam used for illumination. (b) *I–V* characteristics of the device in the dark and in the presence of an illuminating laser with different laser powers. The inset shows the optical image of a monolayer $MoSe_2$ photodetector. (c) Time-resolved photoresponse of the device at a bias voltage of 5 V and a laser power of 0.5 mW mm^{-2}. (d) A single cycle response of laser on and off.

Electrical measurements were performed in the dark and in the presence of an illuminating laser with different powers ranging from 0.1 mW mm^{-2} to 2 mW mm^{-2} (Fig. 5b). The quasilinear *I–V* plots of the device (see inset in Fig. 5b) demonstrate good contact between $MoSe_2$ and the Au electrodes. In contrast to the dark current, the current is significantly increased when the device was illuminated. The *I–V* curves also indicate that the current is strongly dependent on the power of the illuminating laser. At a fixed bias, a larger laser power could lead to a larger current due to the increased number of photon-generated carriers. As a consequence, the photocurrent I_{ph} ($I_{ph} = I_{illuminated} - I_{dark}$) also increases. Photoresponsivity is a critical factor used to evaluate the performance of photodetectors. For the device produced in this study, the effective exposure area is approximately 446 μm^2. At a laser power of 1 mW mm^{-2} and a bias voltage of 10 V, the photoresponsivity is calculated to be approximately 13 mA W^{-1}, which is comparable to the graphene-based photodetector.[59]

Photoresponse time is another critical parameter used to judge device performance. We investigated the time-resolved photoresponse of the device by switching the laser on and off. Fig. 5c shows the current of the device as a function of time at a bias voltage of 5 V and a laser power of 0.5 mW mm^{-2}. The device exhibits a repeatable and stable response to the laser illumination. As the laser is switched on and off, the device shows a low off-state current of ~0.09 nA and a high on-state current of ~1.9 nA, giving a good on/off ratio of ~20. Fig. 5d displays a single cycle response of laser on and off. The measured rise and decay times are ~60 ms, indicating the fast response performance of the device. It should be noted that the performance of the device might be further improved by optimizing the contact or using a phototransistor mode;[57,58] further study is currently underway.

4. Conclusion

In conclusion, a large area of highly crystalline $MoSe_2$ atomic layers has been directly synthesized on SiO_2/Si, mica and Si substrates using a CVD method at atmospheric pressure without the assistance of H_2 gas. Characterization by AFM and Raman confirmed that the thickness of the as-grown $MoSe_2$ ranges from a single layer to a few layers. By using a direct transfer method, we successfully obtained TEM samples. HRTEM together with the SAED pattern demonstrated that the ultrathin $MoSe_2$ flakes are single-crystalline and possess a hexagonal lattice structure. Room-temperature PL indicated that monolayer $MoSe_2$ has a direct bandgap of ~1.56 eV with a strong emission peak. Photodetectors based on monolayer $MoSe_2$ were fabricated and studied for the first time. The devices exhibited a fast response of ~60 ms and a good

photoresponsivity of 13 mA W^{-1}. We believe that this simple CVD approach can be scaled up to produce wafer-scale ultrathin $MoSe_2$ layers on diverse substrates, expanding the applications of this 2D crystal.

Acknowledgements

We gratefully acknowledge financial support from the "Strategic Priority Research Program" of Chinese Academy of Sciences (Grant no. XDA09040203), 973 Project (2012CB932401), National Natural Science Foundation of China (Grant no. 11174362, 91023041, 61390503 and 91323304) and Knowledge Innovation Project of Chinese Academy of Sciences (Grand no. KJCX2-EW-W02).

Notes and references

1 K. S. Novoselov, A. K. Geim, S. V. Morozov, D. Jiang, Y. Zhang, S. V. Dubonos, I. V. Grigorieva and A. A. Firsov, *Science*, 2004, **306**, 666–669.
2 K. S. Novoselov, A. K. Geim, S. V. Morozov, D. Jiang, M. I. Katsnelson, I. V. Grigorieva, S. V. Dubonos and A. A. Firsov, *Nature*, 2005, **438**, 197–200.
3 J. Feng, X. Sun, C. Wu, L. Peng, C. Lin, S. Hu, J. Yang and Y. Xie, *J. Am. Chem. Soc.*, 2011, **133**, 17832–17838.
4 T. Shishidou, A. J. Freeman and R. Asahi, *Phys. Rev. B: Condens. Matter Mater. Phys.*, 2001, **64**, 180401.
5 S. Lei, L. Ge, Z. Liu, S. Najmaei, G. Shi, G. You, J. Lou, R. Vajtai and P. M. Ajayan, *Nano Lett.*, 2013, **13**, 2777–2781.
6 Z. Liu, Y. Gong, W. Zhou, L. Ma, J. Yu, J. C. Idrobo, J. Jung, A. H. MacDonald, R. Vajtai, J. Lou and P. M. Ajayan, *Nat. Commun.*, 2013, **4**, 2541.
7 M. Langer, M. Kisiel, R. Pawlak, F. Pellegrini, G. E. Santoro, R. Buzio, A. Gerbi, G. Balakrishnan, A. Baratoff, E. Tosatti and E. Meyer, *Nat. Mater.*, 2014, **13**, 173–177.
8 Q. H. Wang, K. Kalantar-Zadeh, A. Kis, J. N. Coleman and M. S. Strano, *Nat. Nanotechnol.*, 2012, **7**, 699–712.
9 D. Jariwala, V. K. Sangwan, L. J. Lauhon, T. J. Marks and M. C. Hersam, *ACS Nano*, 2014, **8**, 1102–1120.
10 R. Ganatra and Q. Zhang, *ACS Nano*, 2014, **8**, 4074–4099.
11 S. Z. Butler, S. M. Hollen, L. Cao, Y. Cui, J. A. Gupta, H. R. Gutiérrez, T. F. Heinz, S. S. Hong, J. Huang, A. F. Ismach, E. Johnston-Halperin, M. Kuno, V. V. Plashnitsa, R. D. Robinson, R. S. Ruoff, S. Salahuddin, J. Shan, L. Shi, M. G. Spencer, M. Terrones, W. Windl and J. E. Goldberger, *ACS Nano*, 2013, **7**, 2898–2926.
12 B. Radisavljevic, A. Radenovic, J. Brivio, V. Giacometti and A. Kis, *Nat. Nanotechnol.*, 2011, **6**, 147–150.
13 M. Bernardi, M. Palummo and J. C. Grossman, *Nano Lett.*, 2013, **13**, 3664–3670.
14 R. S. Sundaram, M. Engel, A. Lombardo, R. Krupke, A. C. Ferrari, P. Avouris and M. Steiner, *Nano Lett.*, 2013, **13**, 1416–1421.
15 Z. Yin, H. Li, H. Li, L. Jiang, Y. Shi, Y. Sun, G. Lu, Q. Zhang, X. Chen and H. Zhang, *ACS Nano*, 2012, **6**, 74–80.
16 H. Liu, K. K. A. Antwi, S. Chua and D. Chi, *Nanoscale*, 2014, **6**, 624–629.
17 Y. Chen, J. Xi, D. O. Dumcenco, Z. Liu, K. Suenaga, D. Wang, Z. Shuai, Y.-S. Huang and L. Xie, *ACS Nano*, 2013, **7**, 4610–4616.
18 S. Tongay, D. S. Narang, J. Kang, W. Fan, C. Ko, A. V. Luce, K. X. Wang, J. Suh, K. D. Patel, V. M. Pathak, J. Li and J. Wu, *Appl. Phys. Lett.*, 2014, **104**, 012101.
19 Y. Gong, Z. Liu, A. R. Lupini, G. Shi, J. Lin, S. Najmaei, Z. Lin, A. L. Elias, A. Berkdemir, G. You, H. Terrones, M. Terrones, R. Vajtai, S. T. Pantelides, S. J. Pennycook, J. Lou, W. Zhou and P. M. Ajayan, *Nano Lett.*, 2014, **14**, 442–449.
20 D. Xiao, G. B. Liu, W. X. Feng, X. D. Xu and W. Yao, *Phys. Rev. Lett.*, 2012, **108**, 196802.
21 H. Zeng, J. Dai, W. Yao, D. Xiao and X. Cui, *Nat. Nanotechnol.*, 2012, **7**, 490–493.
22 K. F. Mak, K. He, J. Shan and T. F. Heinz, *Nat. Nanotechnol.*, 2012, **7**, 494–498.
23 J. J. Loferski, *J. Appl. Phys.*, 1956, **27**, 777–784.
24 S. Tongay, J. Zhou, C. Ataca, K. Lo, T. S. Matthews, J. Li, J. C. Grossman and J. Wu, *Nano Lett.*, 2012, **12**, 5576–5580.
25 Z. Y. Zhu, Y. C. Cheng and U. Schwingenschlögl, *Phys. Rev. B: Condens. Matter Mater. Phys.*, 2011, **84**, 153402.
26 Y. Zhang, T.-R. Chang, B. Zhou, Y.-T. Cui, H. Yan, Z. Liu, F. Schmitt, J. Lee, R. Moore, Y. Chen, H. Lin, H.-T. Jeng, S.-K. Mo, Z. Hussain, A. Bansil and Z.-X. Shen, *Nat. Nanotechnol.*, 2014, **9**, 111–115.
27 H. S. S. R. Matte, B. Plowman, R. Datta and C. N. R. Rao, *Dalton Trans.*, 2011, **40**, 10322–10325.
28 S. Larentis, B. Fallahazad and E. Tutuc, *Appl. Phys. Lett.*, 2012, **101**, 223104.
29 J. S. Ross, S. Wu, H. Yu, N. J. Ghimire, A. M. Jones, G. Aivazian, J. Yan, D. G. Mandrus, D. Xiao, W. Yao and X. Xu, *Nat. Commun.*, 2013, **4**, 1474.
30 Y. Y. Peng, Z. Y. Meng, C. Zhong, J. Lu, W. C. Yu, Y. B. Jia and Y. T. Qian, *Chem. Lett.*, 2001, 772–773.
31 J. Pouzet and J. C. Bernede, *Rev. Phys. Appl.*, 1990, **25**, 807–815.
32 D. Kong, H. Wang, J. J. Cha, M. Pasta, K. J. Koski, J. Yao and Y. Cui, *Nano Lett.*, 2013, **13**, 1341–1347.
33 J. Shaw, H. Zhou, Y. Chen, N. Weiss, Y. Liu, Y. Huang and X. Duan, *Nano Res.*, 2014, 1–7, DOI: 10.1007/s12274-014-0417-z.
34 X. Lu, M. I. B. Utama, J. Lin, X. Gong, J. Zhang, Y. Zhao, S. T. Pantelides, J. Wang, Z. Dong, Z. Liu, W. Zhou and Q. Xiong, *Nano Lett.*, 2014, **14**, 2419–2425.
35 X. Wang, Y. Gong, G. Shi, W. L. Chow, K. Keyshar, G. Ye, R. Vajtai, J. Lou, Z. Liu, E. Ringe, B. K. Tay and P. M. Ajayan, *ACS Nano*, 2014, **8**, 5125–5131.
36 J. Yoon, W. Park, G.-Y. Bae, Y. Kim, H. S. Jang, Y. Hyun, S. K. Lim, Y. H. Kahng, W.-K. Hong, B. H. Lee and H. C. Ko, *Small*, 2013, **9**, 3295–3300.
37 J. Liu, Z. Zeng, X. Cao, G. Lu, L.-H. Wang, Q.-L. Fan, W. Huang and H. Zhang, *Small*, 2012, **8**, 3517–3522.
38 Y. Zhou, Y. Nie, Y. Liu, K. Yan, J. Hong, C. Jin, Y. Zhou, J. Yin, Z. Liu and H. Peng, *ACS Nano*, 2014, **8**, 1485–1490.

39 H.-Y. Chang, S. Yang, J. Lee, L. Tao, W.-S. Hwang, D. Jena, N. Lu and D. Akinwande, *ACS Nano*, 2013, **7**, 5446–5452.
40 O. Lopez-Sanchez, E. Alarcon Llado, V. Koman, A. Fontcuberta I Morral, A. Radenovic and A. Kis, *ACS Nano*, 2014, **8**, 3042–3048.
41 L. Britnell, R. M. Ribeiro, A. Eckmann, R. Jalil, B. D. Belle, A. Mishchenko, Y. J. Kim, R. V. Gorbachev, T. Georgiou, S. V. Morozov, A. N. Grigorenko, A. K. Geim, C. Casiraghi, A. H. C. Neto and K. S. Novoselov, *Science*, 2013, **340**, 1311–1314.
42 M. R. Esmaeili-Rad and S. Salahuddin, *Sci. Rep.*, 2013, **3**, 2345.
43 W. Zhang, C.-P. Chuu, J.-K. Huang, C.-H. Chen, M.-L. Tsai, Y.-H. Chang, C.-T. Liang, Y.-Z. Chen, Y.-L. Chueh, J.-H. He, M.-Y. Chou and L.-J. Li, *Sci. Rep.*, 2014, **4**, 3826.
44 W. Regan, N. Alem, B. Alemán, B. Geng, Ç. Girit, L. Maserati, F. Wang, M. Crommie and A. Zettl, *Appl. Phys. Lett.*, 2010, **96**, 113102.
45 Y.-H. Lee, X.-Q. Zhang, W. Zhang, M.-T. Chang, C.-T. Lin, K.-D. Chang, Y.-C. Yu, J. T.-W. Wang, C.-S. Chang, L.-J. Li and T.-W. Lin, *Adv. Mater.*, 2012, **24**, 2320–2325.
46 J.-K. Huang, J. Pu, C.-L. Hsu, M.-H. Chiu, Z.-Y. Juang, Y.-H. Chang, W.-H. Chang, Y. Iwasa, T. Takenobu and L.-J. Li, *ACS Nano*, 2014, **8**, 923–930.
47 Y. Zhang, Y. Zhang, Q. Ji, J. Ju, H. Yuan, J. Shi, T. Gao, D. Ma, M. Liu, Y. Chen, X. Song, H. Y. Hwang, Y. Cui and Z. Liu, *ACS Nano*, 2013, **7**, 8963–8971.
48 S. Wu, C. Huang, G. Aivazian, J. S. Ross, D. H. Cobden and X. Xu, *ACS Nano*, 2013, **7**, 2768–2772.
49 Y.-H. Lee, L. Yu, H. Wang, W. Fang, X. Ling, Y. Shi, C.-T. Lin, J.-K. Huang, M.-T. Chang, C.-S. Chang, M. Dresselhaus, T. Palacios, L.-J. Li and J. Kong, *Nano Lett.*, 2013, **13**, 1852–1857.
50 J. V. Lauritsen, J. Kibsgaard, S. Helveg, H. Topsoe, B. S. Clausen, E. Laegsgaard and F. Besenbacher, *Nat. Nanotechnol.*, 2007, **2**, 53–58.
51 H. R. Gutierrez, N. Perea-Lopez, A. L. Elias, A. Berkdemir, B. Wang, R. Lv, F. Lopez-Urias, V. H. Crespi, H. Terrones and M. Terrones, *Nano Lett.*, 2013, **13**, 3447–3454.
52 T. Liang, W. G. Sawyer, S. S. Perry, S. B. Sinnott and S. R. Phillpot, *Phys. Rev. B: Condens. Matter Mater. Phys.*, 2008, **77**, 104105.
53 A. C. Ferrari and D. M. Basko, *Nat. Nanotechnol.*, 2013, **8**, 235–246.
54 P. N. Ghosh and C. R. Maiti, *Phys. Rev. B: Condens. Matter Mater. Phys.*, 1983, **28**, 2237–2239.
55 P. A. Bertrand, *Phys. Rev. B: Condens. Matter Mater. Phys.*, 1991, **44**, 5745–5749.
56 C. Lee, H. Yan, L. E. Brus, T. F. Heinz, J. Hone and S. Ryu, *ACS Nano*, 2010, **4**, 2695–2700.
57 S. Das, H.-Y. Chen, A. V. Penumatcha and J. Appenzeller, *Nano Lett.*, 2012, **13**, 100–105.
58 O. Lopez-Sanchez, D. Lembke, M. Kayci, A. Radenovic and A. Kis, *Nat. Nanotechnol.*, 2013, **8**, 497–501.
59 T. Mueller, F. Xia and P. Avouris, *Nat. Photonics*, 2010, **4**, 297–301.